

Durham Research Online

Deposited in DRO:

11 May 2015

Version of attached file:

Accepted Version

Peer-review status of attached file:

Peer-reviewed

Citation for published item:

Voïtchovsky, K. and Ashari Astani, N. and Tavernelli, I. and Tetreault, N. and Rothlisberger, U. and Stellacci, F. and Grätzel, M. and Arne Harms, H. (2015) 'In-situ mapping of the molecular arrangement of amphiphilic dye molecules at the TiO₂ surface of dye sensitized solar cells.', *ACS applied materials interfaces*, 7 (20). pp. 10834-10842.

Further information on publisher's website:

<http://dx.doi.org/10.1021/acsami.5b01638>

Publisher's copyright statement:

This document is the Accepted Manuscript version of a Published Work that appeared in final form in *ACS applied materials interfaces*, copyright © 2015 American Chemical Society after peer review and technical editing by the publisher. To access the final edited and published work see <http://dx.doi.org/10.1021/acsami.5b01638>.

Additional information:

Use policy

The full-text may be used and/or reproduced, and given to third parties in any format or medium, without prior permission or charge, for personal research or study, educational, or not-for-profit purposes provided that:

- a full bibliographic reference is made to the original source
- a [link](#) is made to the metadata record in DRO
- the full-text is not changed in any way

The full-text must not be sold in any format or medium without the formal permission of the copyright holders.

Please consult the [full DRO policy](#) for further details.

Article

In-situ mapping of the molecular arrangement of amphiphilic dye molecules at the TiO₂ surface of dye sensitized solar cellsKislon Voitchovsky, Negar Ashari Astani, Ivano Tavernelli, Nicolas Tetreault,
Ursula Rothlisberger, Francesco Stellacci, Michael Grätzel, and Hauke Arne Harms*ACS Appl. Mater. Interfaces*, **Just Accepted Manuscript** • DOI: 10.1021/acsami.5b01638 • Publication Date (Web): 04 May 2015Downloaded from <http://pubs.acs.org> on May 7, 2015**Just Accepted**

“Just Accepted” manuscripts have been peer-reviewed and accepted for publication. They are posted online prior to technical editing, formatting for publication and author proofing. The American Chemical Society provides “Just Accepted” as a free service to the research community to expedite the dissemination of scientific material as soon as possible after acceptance. “Just Accepted” manuscripts appear in full in PDF format accompanied by an HTML abstract. “Just Accepted” manuscripts have been fully peer reviewed, but should not be considered the official version of record. They are accessible to all readers and citable by the Digital Object Identifier (DOI®). “Just Accepted” is an optional service offered to authors. Therefore, the “Just Accepted” Web site may not include all articles that will be published in the journal. After a manuscript is technically edited and formatted, it will be removed from the “Just Accepted” Web site and published as an ASAP article. Note that technical editing may introduce minor changes to the manuscript text and/or graphics which could affect content, and all legal disclaimers and ethical guidelines that apply to the journal pertain. ACS cannot be held responsible for errors or consequences arising from the use of information contained in these “Just Accepted” manuscripts.

1
2
3
4
5
6
7
8
9
10
11
12
13
14
15
16
17
18
19
20
21
22
23
24
25
26
27
28
29
30
31
32
33
34
35
36
37
38
39
40
41
42
43
44
45
46
47
48
49
50
51
52
53
54
55
56
57
58
59
60

In-situ mapping of the molecular arrangement of amphiphilic dye molecules at the TiO₂ surface of dye sensitized solar cells

Kislon Voïtchovsky^{§¶†}, Negar Ashari-Astani^{b†}, Ivano Tavernelli^{b‡}, Nicolas Tétreault[†],

Ursula Rothlisberger^b, Francesco Stellacci[§], Michael Grätzel[†] and Hauke A. Harms^{†}*

§ EPFL STI IMX SUNMIL, Station 12, CH-1015 Lausanne, Switzerland

¶ Physics Department, Durham University, Durham DH1 3LE, United Kingdom

b EPFL SB ISIC LCBC, Avenue F.-A. Forel 2, CH-1015 Lausanne, Switzerland

† EPFL SB ISIC LPI, Station 6, CH-1015 Lausanne, Switzerland

Keywords: atomic force microscopy, dye sensitized solar cells, Z907, molecular dynamics
simulations, liquid phase

1
2
3 ABSTRACT
4
5
6

7 Amphiphilic sensitizers are central to the function of dye-sensitized solar cells. It is known that
8 the cell's performance depends on the molecular arrangement and the density of the dye on the
9 semiconductor surface, but a molecular-level picture of the cell-electrolyte interface is still
10 lacking. Here, we present sub-nanometer *in-situ* atomic force microscopy images of the Z907
11 dye at the surface of TiO₂ in a relevant liquid. Our results reveal changes in the conformation and
12 the lateral arrangement of the dye molecules, depending on their average packing density on the
13 surface. Complementary quantitative measurements on the ensemble of the film are obtained by
14 a quartz-crystal microbalance with dissipation technique. An atomistic picture of the dye
15 coverage-dependent packing, the effectiveness of the hydrophobic alkyl chains as blocking layer
16 and the solvent accessibility is obtained from molecular dynamics simulations.
17
18
19
20
21
22
23
24
25
26
27
28
29
30
31
32
33

34
35 1. Introduction
36
37
38

39 Surface functionalization with self-assembled monolayers (SAMs) is of fundamental
40 importance to nanotechnology, with applications ranging from molecular electronics to
41 controlled wetting, sensing, medical devices and energy harvesting systems.¹⁻⁵ SAM
42 functionalization provides a powerful, yet simple way to manipulate the chemical, electrical and
43 optical properties of surfaces, with the ability to tune the material's macroscopic properties.⁶
44 This is the case for dye-sensitized solar cells (DSCs) where a SAM of dye molecules sensitizes a
45 semiconductor in order to harvest light. DSCs provide a viable alternative to traditional
46 semiconductor solar cells due to their high efficiency and low environmental and industrial
47
48
49
50
51
52
53
54
55
56
57
58
59
60

1
2
3 costs.^{5,7-11} The heart of the DSC is composed of the dye SAM adsorbed on a wide-bandgap
4 semiconductor, usually a high surface area mesoporous TiO₂ photoanode, infiltrated with an
5 electrolyte containing the redox shuttle molecule. The primary role of the dye SAM is to
6 sensitize the TiO₂ semiconductor, similar to sensitization of silver halides in paper photography.
7
8 Upon illumination, the dye goes into a photoexcited state and can inject an electron into the
9 conduction band of the semiconductor. The oxidized dye is regenerated by a hole conductor,
10 traditionally a liquid electrolyte covering the dye and containing a redox mediator. The
11 molecular dye film has also a secondary function: it must act as an electronic barrier that
12 prevents the photoinjected electrons to recombine with the oxidized form of the redox mediator
13 present in the electrolyte. For typical dye molecules, this is ensured by hydrophobic alkyl chains
14 that hinder the redox-mediator from accessing the semiconductor surface, and prevent lateral
15 aggregation of dye molecules. The anchoring groups of the dye, usually carboxylic acids, are
16 hydrophilic, which gives the dye an amphiphilic character and behavior often similar to anionic
17 surfactants. The DSC macroscopic efficiency is known to depend on both the molecular
18 arrangement of the adsorbed dye layer and the contacting electrolyte. This is generally true for
19 most SAM-functionalized surfaces, which requires linking *in-situ* molecular-level details with
20 macroscopic observations in order to derive a full understanding.¹²

21
22
23
24
25
26
27
28
29
30
31
32
33
34
35
36
37
38
39
40
41
42
43
44 Practically, gaining *in-situ* information about the molecular arrangement of dye-sensitizers
45 often proves challenging. Fourier transform infrared spectroscopy was successfully used to
46 observe the binding of dye molecules to the TiO₂ surface of DSCs.^{9,13} The average orientation of
47 adsorbed molecules relative to the surface could be derived from combined near-edge x-ray
48 absorption fine structure spectroscopy (NEXAFS) and photoelectron spectroscopy (PES).¹⁴⁻¹⁶
49
50
51
52
53
54
55
56 However, the irregular mesoporous titania surface prevents averaging techniques from capturing
57
58
59
60

1
2
3 local molecular details. Scanning probe techniques can in principle overcome this difficulty and
4
5 provide direct, local information about the adsorbed layer. Scanning tunneling microscopy
6
7 studies in ultra-high vacuum achieved the first sub-molecular resolution images of the dye layer,
8
9 but the measurements were conducted far from the functional conditions of a DSC.^{17,18} *Ex-situ*
10
11 atomic force microscopy (AFM) results indicated the existence of large dye aggregates on the
12
13 flat TiO₂ substrate for standard device preparation procedure, but molecular resolution was not
14
15 achieved.¹⁹
16
17

18
19
20 Recently developments in the field of AFM have made it possible to achieve sub-nanometer
21
22 mapping of soft and hard surfaces in solution paving the way for *in-situ* local observations of a
23
24 functional DSC's surface.²⁰⁻²²
25
26

27
28 Here we report *in situ* molecular-level AFM images of adsorbed dye molecules at mesoporous
29
30 and flat TiO₂ surfaces in a device-relevant liquid. We used the amphiphilic ruthenium complex
31
32 Z907 (diphenyl-nonyl diphenyl-carboxyl dithio octaruthenium) dye (insert in Figure 2) due to its
33
34 wide-spread use in DSCs, its good performance in long-term stability tests, and the fact that it is
35
36 less prone to aggregation than other dyes.^{23 24} The AFM study is conducted with the sample fully
37
38 immersed either in ethyl-isopropyl sulfone (EiPS), or acetonitrile (MeCN), both solvents being
39
40 used for electrolytes in functional DSCs. We show that under normal conditions, the dye forms a
41
42 single monolayer over the surface. The molecular conformation of the dye depends on the
43
44 density coverage with domains of different molecular conformation able to coexist within the
45
46 adsorbed sub-monolayer. The AFM results are complemented with measurements conducted
47
48 using the quartz crystal microbalance with dissipation technique (QCM-D) so as to assess the
49
50 average quantity of adsorbed molecules on the substrate with respect to coverage saturation. The
51
52 experimental AFM and QCM-D results are supported by molecular dynamics (MD) simulations
53
54
55
56
57
58
59
60

1
2
3 of dyes adsorbed on the (101) facet of anatase TiO_2 immersed in acetonitrile solvent.²⁵⁻²⁷ The
4
5 simulations provide atomic-level insight into the density-dependent changes in the arrangement
6
7 of the adsorbed Z907 molecules.
8
9

10 11 12 13 14 15 2. Methods 16 17

18 19 20 *AFM* 21

22 The AFM data were acquired on a commercial Multimode Nanoscope IIIa (Digital
23 Instruments, now Bruker, Santa Barbara, USA) operated in amplitude-modulation. The sample
24 and the scanning tip were fully immersed into the imaging liquid (ethyl *iso*-propyl sulfone
25 (EiPS), or acetonitrile (MeCN), respectively). Before each experiment, the liquid cell was
26 thoroughly washed in isopropanol and ultrapure water and subsequently dried with nitrogen. We
27 used standard silicon nitride cantilevers (Olympus RC800 PSA, Olympus, Tokyo) with a
28 nominal stiffness of $k_n = 0.76$ N/m. In each experiment the cantilever was driven acoustically
29 with the liquid cell, close to its resonance frequency. Typical imaging amplitudes A were kept
30 between 0.5nm and 1.5nm with the setpoint ratio A/A_0 as large as possible (A_0 is the free
31 vibration amplitude in liquid). The use of relatively soft cantilevers and working amplitudes
32 commensurate with the thickness of the sample-liquid interface allow us to exploit short-range
33 solvation forces so as to enhance the resolution. In these particular imaging conditions, the
34 energy dissipated by the vibrating AFM tip is not sufficient to fully remove the liquid between
35 the tip and the sample, and the tip mainly probes the properties of the interfacial liquid at the
36 surface of the sample.^{12,22,28} The phase contrast is then related to the local ‘wetting’ properties of
37
38
39
40
41
42
43
44
45
46
47
48
49
50
51
52
53
54
55
56
57
58
59
60

1
2
3 the sample, i.e. the local solvation free energy^{12,22} or, at the macroscopic level, the solid-liquid
4 work of adhesion. In practice, imaging over the TiO₂ substrate provides a darker phase contrast
5 than over the Z907 regions, indicating a higher affinity of the solvent for the substrate than for
6 the dye-covered surface (Fig. 3c). If larger imaging amplitudes are used, the phase contrast then
7 reflects mainly the mechanical properties of the sample, but working at large amplitudes is
8 generally detrimental for resolution.²⁸
9
10
11
12
13
14
15
16
17
18
19

20 *QCM-D*

21
22 The quartz microbalance with dissipation technique (QCM-D) directly measures mass uptake
23 on a sensor crystal inside a flow cell. It also allows for simultaneous detection of the viscoelastic
24 properties of the adsorbed molecular layer. In the Q-Sense E4 instrument we are using, the
25 quartz crystal sensor is contacted by gold electrodes, and its sensing side is coated with 67 nm of
26 TiO₂ by the same atomic layer deposition (ALD) process that is used for coating the silicon
27 substrates used for AFM measurements. The sensor is placed into a flow cell where its TiO₂ side
28 can be exposed to liquid dye solution in order to measure mass change in situ. Given the
29 molecular weight of the Z907 dye molecule, the QCM-D technique is sensitive enough to
30 quantify sub-monolayers of adsorbed molecules on flat TiO₂ film, see Harms *et al.*²⁷ for details.
31
32
33
34
35
36
37
38
39
40
41
42
43
44
45

46 *Computational methods*

47
48 Classical molecular dynamics (MD) simulations were performed for different dye coverage
49 and various packing modes and orientations. The TiO₂ surface was described by the Bandura
50 Kubicki force field, whereas for the Z907 dye a force field was developed following the AMBER
51 protocol.²⁹⁻³¹ Classical point charges were derived using the RESP procedure except for the
52
53
54
55
56
57
58
59
60

1
2
3 carboxylic anchoring groups, whose charges were chosen in such a way as to reproduce the
4 experimental adsorption energy.^{32,33} For this purpose we used the Gaussian 09 Package.³⁴ The
5 force field was validated via full *ab initio* simulations of a single dye in vacuum. A united atom
6 OPLS force field was employed for acetonitrile.³⁵
7
8
9
10
11

12 Experimental and computational studies have suggested different binding modes for Z907 and
13 similar dyes.^{9,36-38} Initial tests showed that the different binding modes (dissociative, bidentate,
14 or monodentate) hardly affect the space occupied by each dye and hence have little influence on
15 the overall packing geometries. For all studies presented here, we thus have adopted a single,
16 non-dissociative bidentate binding mode.
17
18
19
20
21
22
23

24 Initial models of the system composed of two layers of anatase TiO₂ (108×113 Å² for low and
25 medium coverage and 54×56 Å² for high coverage) were constructed using Materials Studio.³⁹
26 Molecular dynamics simulations were performed with the Amber12 package using the PMEMD
27 module.²⁹
28
29
30
31
32
33

34 Production runs of about 20 ns in the NVE ensemble were sampled after initial minimization
35 and 5 ns of equilibration in the canonical ensemble using Nose-Hoover thermostats at room
36 temperature (300 K).
37
38
39
40
41
42

43 *Sample preparation*

44 TiO₂ samples for AFM measurements were based on a (100) silicon wafer substrate coated
45 with titanium dioxide by atomic layer deposition from a tetrakis(dimethylamino)titanium
46 (TDMAT) precursor as described previously.⁴⁰ The TiO₂ film of 67 nm thickness was annealed
47 at 420°C and had a surface roughness of ~2.0 nm on a 4 μm AFM frame. X-ray diffraction of the
48 film showed evidence of anatase crystallites but no rutile phase, see supporting information. The
49
50
51
52
53
54
55
56
57
58
59
60

1
2
3 Z907 pigment was dissolved in a 1:1 volumetric mixture of *tert*-butanol and acetonitrile, and a
4
5 solution of 50.0 μM concentration was quantified by an absorption measurement using the
6
7 published extinction coefficient of $12200 \text{ M}^{-1}\text{cm}^{-1}$; lower concentrations were obtained by
8
9 dilution.²³
10

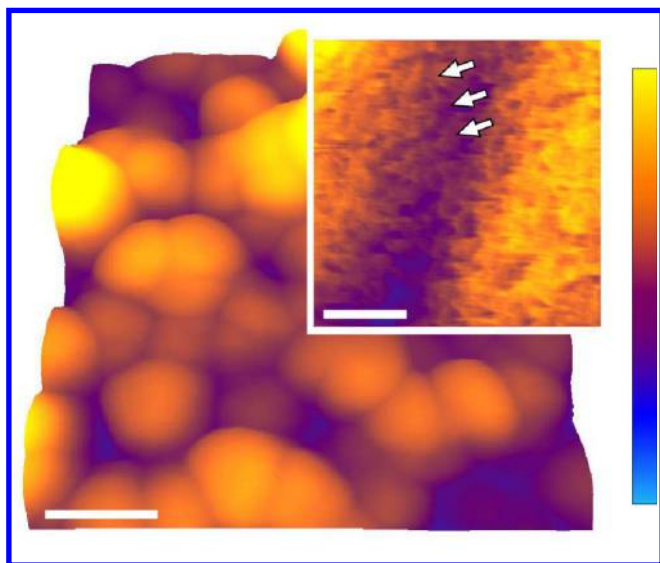
11
12 Prior to staining, the AFM substrates were cleaned by UV-ozone for 10 min and subsequently
13
14 heated for 30 min at 420°C to remove organic residuals and excess water from the TiO_2 surface.
15
16 After cooling down to 70°C they were immersed into the dye solution for 30 min, rinsed in
17
18 ${}^t\text{BuOH}:\text{MeCN}$ mixture, immersed in MeCN for 30 min, stained again for 10 min, rinsed in
19
20 ${}^t\text{BuOH}:\text{MeCN}$ mixture, immersed in MeCN for 30 min, stained again for 10 min, rinsed in
21
22 ${}^t\text{BuOH}:\text{MeCN}$ mixture and MeCN, and subsequently stored in MeCN in the dark.
23

24
25 Samples destined for AFM measurements were usually transferred to EiPS as an imaging
26
27 liquid. EiPS is a main constituent in non-volatile high-voltage electrolytes that are used in
28
29 industrial applications of dye sensitized solar cells.^{41,42} EiPS was chosen for its relevance in DSC
30
31 applications and for its low vapor pressure (compared to MeCN) making it is easier to reach
32
33 stable imaging conditions at high resolution. Aside from experimental considerations, no
34
35 differences could be seen in the images obtained in MeCN and EiPS (see supporting information
36
37 Figure S1).
38
39

40 41 42 43 3. Results 44 45 46 47

48
49 **Figure 1** presents a high-resolution image of the surface of a DSC in a functionally relevant
50
51 liquid. The measurement, conducted with AFM in EiPS, provides a unique insight into the sub-
52
53 nanometer details of the device's surface and indicates some structure in the dye layer. The dye
54
55 molecules appear to be arranged along some preferential directions (arrows in the inset) although
56
57
58
59
60

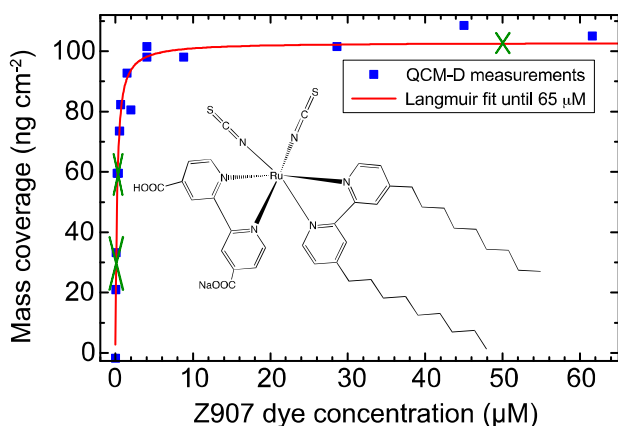
1
2
3 no long-range order is visible. These results should however be taken cautiously due to the high
4
5 surface curvature of mesoporous TiO_2 which renders AFM imaging challenging due to tip-
6
7 convolution effects. An additional difficulty arises from the fact that dye molecules tend to
8
9 accumulate primarily in holes and surface groves at intermediate coverage, making a study of the
10
11 dye molecular arrangement as a function of surface coverage difficult.
12
13



14
15
16
17
18
19
20
21
22
23
24
25
26
27
28
29
30
31
32
33
Figure 1. High-resolution AFM image of the surface of a DSC in liquid. The surface is
34
35 composed of mesoporous TiO_2 stained with the Z907 ruthenium dye. The TiO_2 nanoparticles are
36
37 clearly visible in the main image. The inset shows molecular detail of the dye arrangement at the
38
39 edge of a nanoparticle with some ordering visible (arrows). The scale bars are 40 nm (main
40
41 image) and 3 nm (inset). The colour scale is 70 nm (main image) and 6 nm (inset).
42
43
44
45
46
47
48

49 To overcome these difficulties, we have used flat TiO_2 substrates throughout this study. The
50
51 substrates, obtained by atomic layer deposition, present a sufficiently low roughness on the
52
53 nanoscale to avoid ambiguous interpretation of the AFM results. For each sample, the actual
54
55 surface coverage is determined by QCM-D so as to ensure that the local AFM observations
56
57
58
59
60

1
2
3 reflect global surface properties. The adsorption behavior of the same Z907–TiO₂ system has
4 previously been studied by using a QCM-D.²⁷ **Figure 2** shows the adsorption isotherm for Z907
5 on flat TiO₂ films. The figure uses previously published data²⁷ as a reference for comparison
6 with the current measurements. The isotherm follows a Langmuir-type behavior (red line),
7 indicating a saturation value of 103 ng cm⁻² area mass uptake over the concentration range on
8 display. This corresponds to 0.76 molecules/nm², or a molecular footprint of 1.31 nm²/molecule
9 when assuming a flat surface. We define this saturation value as 100 % mass coverage, which
10 should correspond to a densely packed monolayer of Z907. For staining the AFM samples, dye
11 concentrations were chosen such that a mass coverage of approximately 30 %, 60 % or 100 %
12 concentrations were chosen such that a mass coverage of approximately 30 %, 60 % or 100 %
13 was obtained (green data crosses in Figure 2).
14
15
16
17
18
19
20
21
22
23
24
25
26
27



28
29
30
31
32
33
34
35
36
37
38
39
40
41
42
43
44
45 **Figure 2.** QCM-D area mass uptake over concentration of sensitizing dye solution with a
46 Langmuir isotherm fitted to the data. Blue data points are taken from previously published
47 experiments²⁷. Green crosses mark the three concentrations of dye solutions used for staining
48 the AFM samples and indicate their corresponding mass coverage. The insert shows the structure
49 of the Z907 ruthenium dye.
50
51
52
53
54
55
56
57
58
59
60

1
2
3 A representative AFM topographic image of the flat TiO₂ surface after sensitization with dye
4 molecules (30 % mass coverage) is shown in **Figure 3a**. The image shows large protrusions (20-
5
6 molecules (30 % mass coverage) is shown in **Figure 3a**. The image shows large protrusions (20-
7
8 30 nm wide, and ~2 nm high) that are related to the roughness of the TiO₂ substrate. Details of
9
10 the dye molecules are already visible, appearing as a sub-nanometer, mostly homogeneous
11
12 roughness on the surface. This is confirmed in higher magnification images of the sample where
13
14 the dye film appears as homogenous sponge-like structure (inset in Figure 3a). Using harsh
15
16 imaging conditions, it is possible to mechanically remove dye molecules in selected regions by
17
18 scratching. The scratched region, which corresponds to the TiO₂ substrate, appears darker in the
19
20 phase image (purple arrow in Figure 3b and c). This phase contrast indicates a higher affinity of
21
22 the solvent for the TiO₂ than for the dye, and could be consistently used throughout this study to
23
24 identify dye-covered (light) and uncovered (dark) regions.^{12,22} At 30 % mass coverage, the dye
25
26 layer exhibits dark spots in the phase, suggesting that uniform gaps exist between the adsorbed
27
28 Z907 molecules. These gaps give the apparent sponge-like appearance to the dye layer
29
30 topography. The thickness of the dye film is difficult to evaluate directly from Figure 3a due to
31
32 the roughness of the substrate. It is however possible to use the exposed TiO₂ region as a
33
34 reference. A line profile taken at the edge of the dye layer indicates a thickness of ~0.6 nm
35
36 (Figure 3d). This value is a lower estimate of the real thickness due to the mechanical
37
38 perturbation induced by the AFM tip on the dye molecules during the imaging process.
39
40
41
42
43
44
45
46
47
48
49
50
51
52
53
54
55
56
57
58
59
60

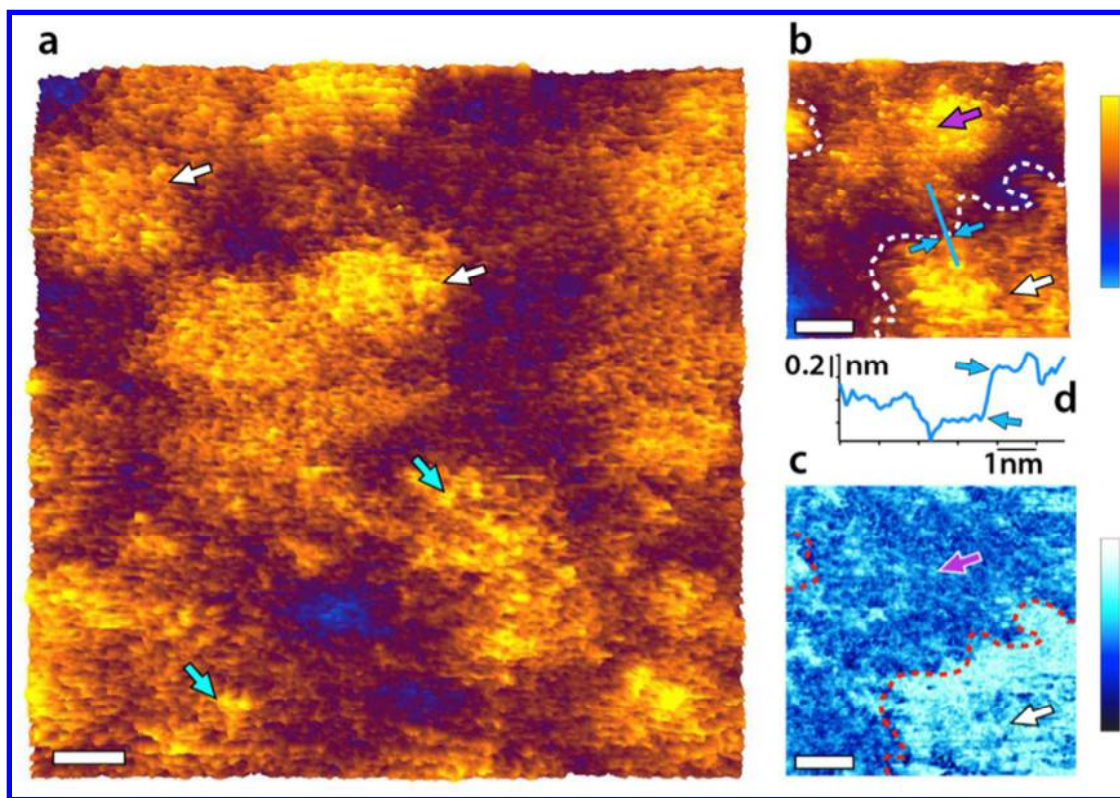


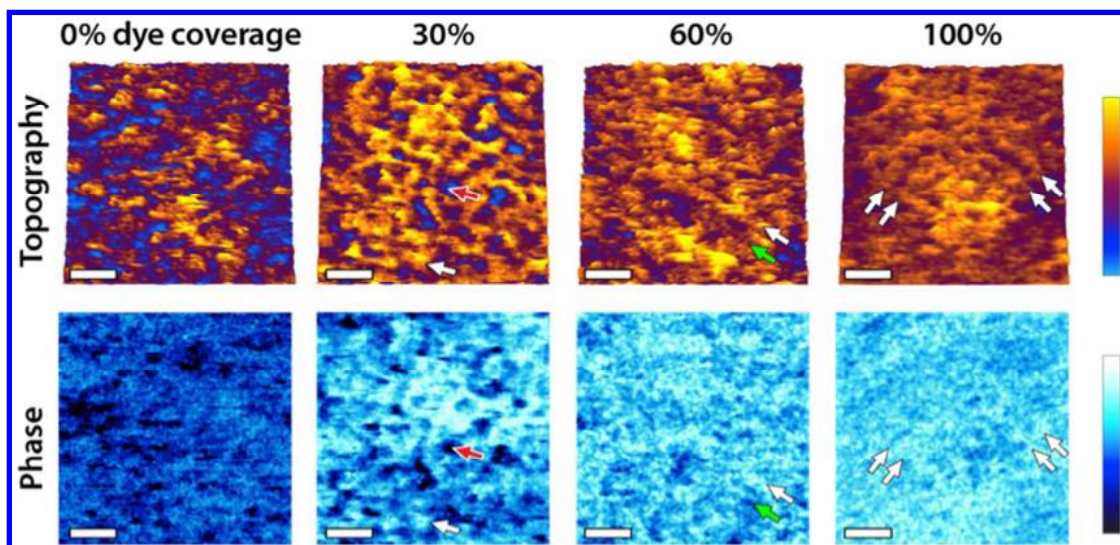
Figure 3. AFM micrographs of a TiO₂ surface covered with Z907 ruthenium dye (30 % mass coverage). (a) A low magnification (100 nm) topographic image shows almost uniform coverage by the dye apart for a few higher dye domains (blue arrows). The ~ 20 nm wide protrusions (white arrows) are related to the substrate roughness. Higher resolution topographic (b) and phase (c) images of the surface reveal a sponge-like structure of the dye layer (white arrow). The substrate can also be exposed by scratching with the AFM tip (b-c) revealing a ~ 0.6 nm dye layer thickness. The exposed TiO₂ substrate (purple arrow) exhibit a clear phase contrast (dotted red line) with the lighter Z907 domains. A topographic profile (d) taken over the TiO₂-Z907 border (blue line in b) indicates a thickness of ~0.4 nm for the Z907 dye layer. The topographic images are always represented with an orange-blue color scale and the phase images in blue-black throughout the paper. The scale bars are 10 nm (a) and 3 nm (b, c). The colour bars are 3 nm (a, b) and 15° (c).

1
2
3
4
5
6 A closer look at Figure 3a reveals occasional variations in height of the dye layer over flat
7
8 substrate regions (blue arrows). These regions hint to local variations of the Z907 molecular
9
10 arrangement on the substrate surface, which could be related to the density of dye molecules. In
11
12 order to examine this effect in a systematical manner, we acquired high-resolution AFM images
13
14 of the dye layer at different mass coverage, as determined by QCM-D.
15
16

17
18 Representative AFM images are presented in **Figure 4** for 0 %, 30 %, 60 % and 100 % mass
19
20 coverage. A clear trend is visible in both the topography and the phase with the increase of dye
21
22 coverage. The bare substrate (0 %) appears relatively rough, the image is noisy and provides
23
24 little phase contrast. At 30 % mass coverage, 1-3 nm wide dye features are visible in both
25
26 topography and the phase, and form a soft sponge-like layer probably templated by the atomic
27
28 structure of the TiO₂ substrate. From the phase image, the holes (red arrow) can be attributed to
29
30 the substrate while the top of the layer is due to dye molecules and appear already more regular
31
32 and smoother than raw substrate (white arrow). At 60 % mass coverage, the layer is more
33
34 ordered and appears in an intermediate situation with the dye molecules forming both rows
35
36 (white arrow) and lower, less ordered regions (green arrow). The fully covered surface appears
37
38 smooth with little height variations. The whole surface is covered in row-like domains, which are
39
40 not necessarily aligned (arrows). The phase image becomes consistently brighter as the surface
41
42 coverage increases, indicating the substrate is fully covered at 100 % mass coverage.
43
44
45
46
47

48
49 Interestingly, the dye molecules always spread over all the space available and never form
50
51 isolated islands. At 10 % mass coverage, the spreading of the dye molecules prevented non-
52
53 destructive imaging (not shown).
54
55
56
57
58
59
60

1
2
3 The AFM results suggest a change in the molecular arrangement of the dye molecules on the
4 surface as the dye coverage increases. The coexistence of two height levels at intermediate
5 coverage supports this explanation. The formation of dye rows at higher coverage (also visible in
6 MeCN, see supplementary Figure S1) is consistent with the observations on the mesoporous
7 TiO₂ (Figure 1) and coincide with an increased layer thickness, suggesting that the Z907
8 molecules sit with their alkyl chains extended away from the substrate surface when arranged in
9 rows (Figure 7). This interpretation would also explain the increased surface density of dye at
10 higher mass coverage, especially given the fact that the dye molecules spread over the whole
11 available TiO₂ at all coverage conditions.
12
13
14
15
16
17
18
19
20
21
22
23
24
25
26



27
28
29
30
31
32
33
34
35
36
37
38
39
40
41
42
43
44
45 **Figure 4.** High-resolution AFM images of the dye layer at 0 %, 30 %, 60 % and 100 % mass
46 coverage obtained in similar imaging conditions. At 0 % the substrate appears rough and noisy
47 due to short-range tip-sample attractive interactions. At 30 %, the dye molecules (white arrow)
48 assemble in a soft sponge-like disordered structure that can easily be disrupted by the AFM tip.
49
50
51
52
53
54
55
56
57
58
59
60
Multiples holes are visible in the layer (red arrow) and appear darker in the phase. At 60 %, the
layer is partially ordered with the apparition of rows (white arrow) and less ordered lower

1
2
3 regions (green arrow). At 100 % the surface is fully covered, it appears smooth and only dye
4 rows are visible (white arrows). The scale bar is 2 nm and the colour scales are 1 nm
5
6
7 (topography) and 15° in all images.
8
9

10
11
12
13 To further explore the atomistic arrangement of the dye film on the TiO₂ surface, we
14 performed molecular dynamics (MD) simulations at different dye densities. 100 % mass
15 coverage was simulated using a density of 0.76 molecules/nm² as obtained from QCM-D
16 measurements. The dye molecules were arranged on a crystalline anatase (101) TiO₂ slab with
17 two layers. Possible binding locations were identified based on geometric arguments: using an
18 approximate distance between the two carboxylic groups of a bipyridine moiety of ca. 7 Å as a
19 gauge, we tried to find adsorbing sites on the substrate with the same distance. Five possible
20 locations were identified, as displayed in **Figure 5**. The same 5 locations were confirmed by
21 random adsorption simulations where dyes initially located at 10-15 Å distance from the surface
22 in vacuum were allowed to adsorb randomly during the first nanosecond of the simulation. For
23 each of the five binding locations, a regular system of 25 dyes adsorbed on the titanium oxide
24 surface was constructed. After minimization, the lowest energy configuration (Site 1 in **Table 1**)
25 was chosen for conducting further simulations to study the effect of coverage density on packing.
26
27
28
29
30
31
32
33
34
35
36
37
38
39
40
41
42
43

44 As a further validation, we performed annealing simulations of all 5 systems, in which the
45 temperature was raised to 600 K followed by cooling down to low temperatures. Consistent with
46 the relative energetics shown in Table 1, dyes located in the energetically most stable site 1
47 arrangement remained at their binding sites, whereas other configurations went through several
48 transitions between different arrangements, (for configurations with sites 5, 2, and 4) and
49 occasionally detached from the surface (in the case of site 3). An additional parameter that
50
51
52
53
54
55
56
57
58
59
60

strongly influences the energetics of the packing is the orientation of the dye. For instance in the most stable orientation for site 1, the sulfur atoms are inversely aligned along the $[10\bar{1}]$ direction, whereas the opposite orientation is less stable (see supporting information Figure S2).

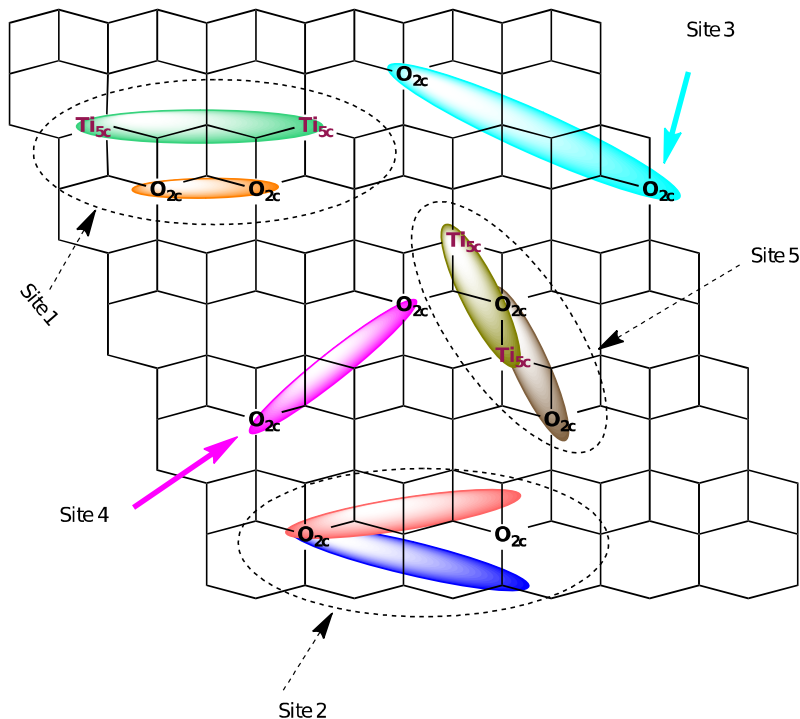


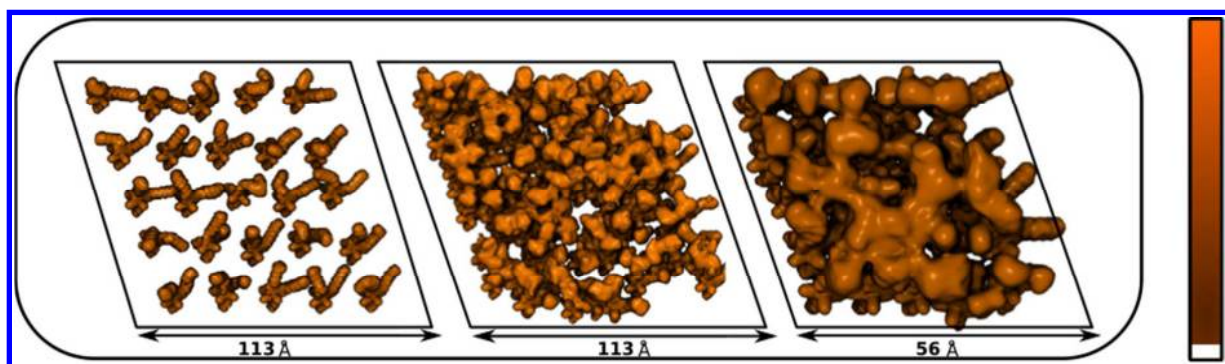
Figure 5. Five possible location sites suitable for simultaneous anchoring of the carboxygroups of the bipyridine moiety. The Z907 dye always occupies roughly the same (dotted) area in sites 1, 2 and 5, regardless of the selected binding mode inside the ellipse. For site 1, Z907 in its fully protonated structure can make hydrogen bonds with two 2-coordinated oxygens (O_{2c}). In its deprotonated state, the bipyridine moiety can make bonds to 5-coordinated Ti (Ti_{5c}), either way occupying the same space shown in dots. The same holds true for site 5. For site 2, the bipyridine can be in the salmon-colored ellipse or the blue one, either way making hydrogen bonds to the same two ridge oxygens indicated.

Table 1. Relative energetics for different dye location sites, as displayed in Figure 5, evaluated for a system composed of 25 dyes. The relative energetics was evaluated for a 33% mass coverage system where dye-dye interactions are less important.

Adsorption site	Relative energetics [kcal/mol dye molecule]
Site 1	0
Site 2	15.4
Site 3	25.6
Site 4	30.8
Site 5	48.7

In order to visualize the effect of dye coverage on the conformation of the dye layer, we computed a topographic picture of the system comprising 25 dye molecules averaged over 20 ns of simulation (**Figure 6**), comparing 33 % mass coverage ($0.23 \text{ molecules nm}^{-2}$), 66 % mass coverage ($0.51 \text{ molecules nm}^{-2}$) and 100 % mass coverage ($0.76 \text{ molecules nm}^{-2}$). In order to change the mass coverage in the computations, the size of the TiO_2 slab was adjusted accordingly, while the number of dye molecules was kept constant. At lower densities, one of the lipophilic alkyl chains is mostly extended parallel to the surface whereas the other is pointing upwards (**Figure 7**). This leads to a configuration where the dyes are packed closer to the surface, i.e. the average layer distance is ca. 8.7 \AA with an average tilting angle of $38^\circ \pm 6^\circ$ of the bipyridine moiety with respect to the titanium oxide surface. Figure 7 shows that for 100 % dye coverage, the atomic density profile along the z direction has a shoulder around 13 \AA and the

1
2
3 probability to find dye atoms (mostly from the alkyl chains) in this range (13-25 Å) is higher
4
5 than the one of the 33 % mass coverage system (bottom graph in Figure 7). In fact, at higher
6
7 densities (66 % and 100 %), both alkyl chains of each dye molecule start to be oriented vertically
8
9 with respect to the TiO₂ surface with average dye-layer thicknesses of approximately 9.00 Å and
10
11 10.2 Å and an average tilting angle of 42°± 3° and 55°± 3°, respectively (Figure 7-note that
12
13 instantaneous tilting angles shown in the figure for one snapshot are not necessarily identical to
14
15 the average values).
16
17
18
19
20
21
22
23
24
25
26



38
39 **Figure 6 .** The simulated AFM pictures for different mass coverage (33%, 66%, and 100% from
40
41 left to right, respectively). Map of the weighted atomic density of dye molecules. The map is
42
43 done by replacing each dye atom with a normalized Gaussian distribution of width (standard
44
45 deviation) equal to the atomic radius. The Gaussian distribution for each atom is then weighted
46
47 with the occupancy. The various Gaussians are added and distributed on a grid (orange color).
48
49 The isosurface value is 0.01. The same map with restriction to the parts of dye molecules that are
50
51 13-25 Å away from the TiO₂ surface is shown in the supporting information Figure S7.
52
53
54
55
56
57
58
59
60

1
2
3 As the experimental results in this AFM study and in other STM studies³⁷ suggest, the TiO₂
4 surface templates the dye arrangement via the binding site, and the packing is less driven by dye-
5 dye interactions in terms of energy. Simulations results for the low coverage system (less dye-
6 dye interactions) also show significant energy differences between different dye arrangements on
7 the TiO₂ template (Table 1). AFM nanographs at 60 % mass coverage suggest the possible
8 coexistence of distinct domains of dye molecules with the alkyl chains either pointing away from
9 the surface, or stretched out along the surface. Indeed our MD simulations results also reflect the
10 coexistence of quasi parallel and quasi vertical alkyl chains and also show that the relative
11 population of the two alkyl chain orientations is density dependent (Figure 7). At low coverage
12 one alkyl chain is mostly parallel and one vertical while at high coverage both alkyl chains are
13 found in a quasi vertical configuration. The intermediate coverage consists of a mixture of dye
14 molecules with these two main configurations. For this intermediate coverage range, we also
15 explored few inhomogeneous configurations with dye domain formation (supporting information
16 Figure S3).

17
18
19
20
21
22
23
24
25
26
27
28
29
30
31
32
33
34
35
36 In addition, we analyzed the solvent accessibility of the SAM (supporting information Figure
37 S4). For all three coverages, the dye molecules reduce the accessibility of the solvent to the TiO₂
38 with respect to a dye-free surface (left side on Figure S4). This solvent screening sets in at farer
39 distances and is more effective for higher coverage where alkyl chains are positioned more
40 vertically and the monolayer thickness is larger.
41
42
43
44
45
46
47
48
49
50
51
52
53
54
55
56
57
58
59
60

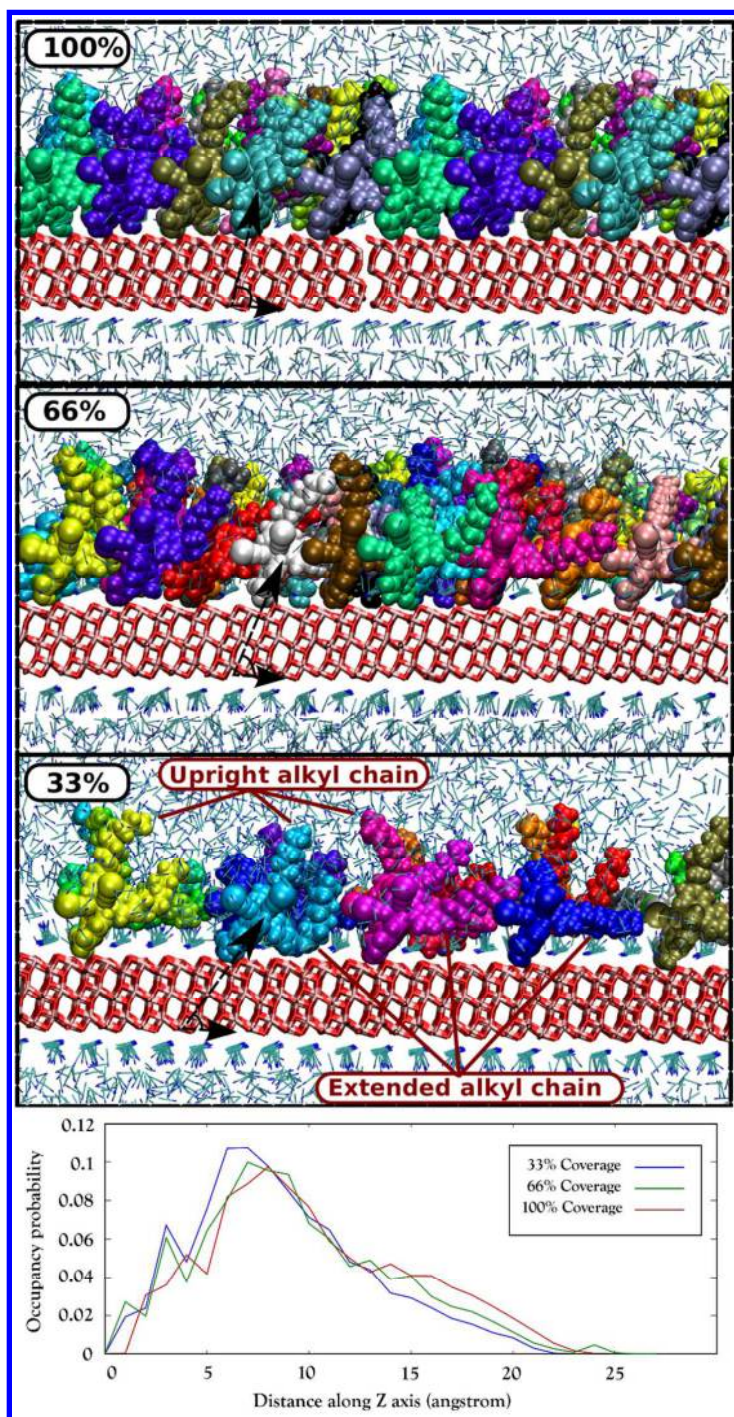


Figure 7. Side view of the three systems with different mass coverage. The tilting angle is indicated with black arrows. When going to higher mass coverage (top pictures), more alkyl chains assume an upright position. Lower part: The probability of finding dye atoms along the Z-axis (normal to the surface) for 20 ns of MD simulation in NVE ensemble.

1
2
3
4
5
6 Besides the conformational change of the alkyl chains with respect to the surface, MD
7
8 simulations at nominal 100 % dye coverage also indicate that the binding location of the
9
10 molecules close to maximum coverage can be altered. In the areas with densely packed
11
12 arrangements, dyes encumber each other forcing their neighbors to take positions, which are not
13
14 usually energetically preferred (in terms of adsorption sites and can even detach from the surface
15
16 at higher temperatures (supporting information Figure S5).
17
18
19
20
21

22 4. Discussion 23 24 25 26

27 Results from AFM measurements and MD computations both indicate that the amphiphilic
28
29 Z907 dye covers most of the TiO₂ surface already at 33 % mass coverage by stretching out its
30
31 alkyl chains along the TiO₂ surface. For 100 % weight coverage, experiment and simulation
32
33 show that the molecules form a densely packed monolayer, with both alkyl chains adapting an
34
35 upright conformation. This microscopic observation confirms the common understanding that
36
37 alkyl chains can shield the TiO₂ surface in applications like dye sensitized solar cells and it
38
39 elucidates the way in which they do.
40
41
42

43 Our observation of two different types of conformation of the dye molecules matches well with
44
45 previous findings on anisotropic dye molecules by combined NEXAFS and PES studies;^{16,43} our
46
47 measurement offers an independent confirmation by a direct and complementary AFM
48
49 observation in an actually relevant liquid environment. The existence of two adsorbed
50
51 conformations is reminiscent of the well-known ‘flat lying’ and ‘standing’ molecular
52
53 configurations of alkanethiols SAMs on gold.⁴⁴ The analogy with the present case is nonetheless
54
55
56
57
58
59
60

1
2
3 not obvious given the important differences in the type of bond formed between the dye and the
4
5 substrate.
6

7
8 Our measurements also provide high-resolution lateral information, i.e. conformity and
9
10 homogeneity of the film at high mass coverage. Considering the amphiphilic nature of the Z907
11
12 molecule, these findings could remain valid for surfactant adsorption at low concentration in
13
14 general.
15

16
17 In the particular case of dye sensitized solar cells, the staining of mesoporous TiO₂ is carried
18
19 out at high Z907 dye concentration (250 μM). However, it is known that it takes several hours
20
21 for the dye to reach the bottom of a mesoporous film, and even longer to fully saturate the dye
22
23 uptake in the mesoporous film.^{45,46} This indicates that during the staining process, all of the
24
25 different conformations and different degrees of mass coverage are present in part of the
26
27 mesoporous TiO₂ film. This implies that the results derived by QCM-D and AFM on flat model
28
29 systems provide meaningful insights that are relevant to the mesoporous system. In particular,
30
31 amphiphilic sensitizers can effectively cover the TiO₂ surface already at low mass coverage, so
32
33 the shielding of the TiO₂ from the electrolyte can be effective even if the staining of deeper
34
35 layers of the mesoporous TiO₂ film is incomplete. Practically, this would result in a working
36
37 device with good fill factor and photovoltage, but the photocurrent would be inferior to a similar
38
39 device in which 100% dye mass coverage was achieved. On both, flat and mesoporous TiO₂, we
40
41 consistently observe monolayers of Z907, not agglomerations, as earlier AFM reports of lower
42
43 resolution suggest.¹⁹ We observed dye agglomerations only upon special sample preparation
44
45 procedures, e.g. when the rinsing of the sample was omitted. Furthermore, the existence of
46
47 molecular rows could be observed on both the flat and the mesoporous substrate by AFM in
48
49 EiPS, supporting the generality of our findings in different electrolytes. The observation of two
50
51
52
53
54
55
56
57
58
59
60

1
2
3 different conformations is in fact further supported by the two-step adsorption kinetics that are
4 often observed in DSCs.^{27,47}
5
6

7
8 In the more general sense, it is very encouraging that the computational method produces good
9 agreement with the results of the AFM study. The MD simulation only used the quantitative
10 input on the number of dye molecules per area, as obtained experimentally from the QCM-D
11 mass coverage. Computations then produced a detailed description of the adsorbed molecular
12 film in liquid environment, which corresponds very well to the experimental data obtained
13 independently by AFM. The AFM study presented in this paper is at the limit of the resolution
14 that can currently be achieved on molecular films in a relevant liquid environment, but the model
15 at the basis of the MD simulation may still describe the behavior of molecular films correctly at a
16 level that is beyond the resolution of current experimental methods.
17
18
19
20
21
22
23
24
25
26
27
28
29
30

31 5. Conclusion

32
33
34
35

36 In this study we have combined high-resolution AFM, QCM-D and MD simulations to
37 elucidate the molecular arrangement of the Z907 dye molecules at the surface of TiO₂ in a
38 functionally relevant liquid. Our results detail the formation of the dye monolayer, showing
39 several molecular conformations on the surface at different dye concentration.
40
41
42
43
44

45 Future work will address molecular films that consist of functional molecules coadsorbed with
46 chelating agents such as bile acids, e.g. porphyrin sensitizers and cheno deoxycholic acid, where
47 the nature of interaction and the arrangement of dye and coadsorbate within the sensitizing film
48 still wait to be unveiled.
49
50
51
52
53
54
55
56
57
58
59
60

1
2
3 **Supporting Information.** High-resolution AFM image of the Z907 dye layer in acetonitrile.
4
5 orientation with respect to the crystal lattice of packing, calculated solvent density along the z
6
7 axis (vertical to the TiO₂ slab). This material is available free of charge via the Internet at
8
9 <http://pubs.acs.org>
10
11

12 13 14 **Corresponding Author**

15
16 * hauke.harms@alumni.epfl.ch
17
18

19 20 **Current Address**

21
22 † I.T. moved to IBM Research GmbH, Zurich Research Laboratory, 8803 Rueschlikon,
23
24 Switzerland.
25
26

27 28 **Author Contributions**

29
30
31 The manuscript was written through contributions of all authors. All authors have given approval
32
33 to the final version of the manuscript. ‡These authors contributed equally.
34
35
36

37 38 **Funding Sources**

39
40 K.V. acknowledges funding from the Swiss National Science Foundation through the
41
42 Ambizione Fellowship (PZ00P2_136941). U.R. acknowledges funding from the Swiss National
43
44 Science Foundation via individual grant No. 200020-146645 and the NCCRs MUST and
45
46 MARVEL and also acknowledges support from the Swiss National Computing Center (CSCS)
47
48 and the CADMOS project for computing resources. M.G. thanks the European Research Council
49
50 (ERC) for supporting part of this work under the advanced research grant (no. 247404)
51
52 MESOLIGHT. H.A.H. acknowledges funding from the Swiss National Science Foundation
53
54
55
56
57
58
59
60

1
2
3 (SNF). M.G. and N.T. acknowledge funding from the King Abdullah University of Science and
4
5
6 Technology (KAUST, Award no. KUS-C1-015-21).
7

8
9 ACKNOWLEDGMENT

10
11 We thank S. M. Zakeeruddin for providing the Z907 dye and EiPS.
12
13
14
15
16

17
18 REFERENCES

19
20
21
22 (1) Akkerman, H. B.; Blom, P. W. M.; de Leeuw, D. M.; de Boer, B. Towards Molecular
23
24 Electronics with Large-Area Molecular Junctions. *Nature* **2006**, *441*, 69–72.
25
26

27
28 (2) Bain, C. D.; Whitesides, G. M. Correlations Between Wettability and Structure in
29
30 Monolayers of Alkanethiols Adsorbed on Gold. *J. Am. Chem. Soc.* **1988**, *110*, 3665–3666.
31
32

33
34 (3) Flink, S.; Van Veggel, F.; Reinhoudt, D. N. Sensor Functionalities in Self-Assembled
35
36 Monolayers. *Adv. Mater.* **2000**, *12*, 1315-1328.
37

38
39 (4) Langer, R.; Tirrell, D. A. Designing Materials for Biology and Medicine. *Nature* **2004**,
40
41 *428*, 487–492.
42
43

44
45 (5) O'Regan, B.; Grätzel, M. A Low-Cost, High-Efficiency Solar Cell Based on Dye-
46
47 Sensitized Colloidal TiO₂ Films. *Nature* **1991**, *353*, 737–740.
48
49

50
51 (6) Love, J. C.; Estroff, L. A.; Kriebel, J. K.; Nuzzo, R. G. Self-Assembled Monolayers of
52
53 Thiolates on Metals as a Form of Nanotechnology. *Chem. Rev.* **2005**, *105*, 1103-1169.
54
55
56
57
58
59
60

1
2
3 (7) Hagfeldt, A.; Boschloo, G.; Sun, L.; Kloo, L.; Pettersson, H. Dye-Sensitized Solar Cells.
4
5 *Chem. Rev.* **2010**, *110*, 6595–6663.
6

7
8 (8) Han, L.; Islam, A.; Chen, H.; Malapaka, C.; Zhang, S.; Yang, X.; Yanagida, M. High-
9
10 Efficiency Dye-Sensitized Solar Cell with a Novel Co-Adsorbent. *Energy Environ. Sci.* **2012**, *5*,
11
12 6057-6060.
13
14

15
16 (9) Gao, F.; Wang, Y.; Shi, D.; Zhang, J.; Wang, M.; Jing, X.; Humphry-Baker, R.; Wang,
17
18 P.; Zakeeruddin, S. M.; Grätzel, M. Enhance the Optical Absorptivity of Nanocrystalline TiO
19
20 2Film with High Molar Extinction Coefficient Ruthenium Sensitizers for High Performance
21
22 Dye-Sensitized Solar Cells. *J. Am. Chem. Soc.* **2008**, *130*, 10720–10728.
23
24
25

26
27 (10) Grätzel, M. The Advent of Mesoscopic Injection Solar Cells. *Prog. Photovolt: Res. Appl.*
28
29 **2006**, *14*, 429–442.
30
31

32
33 (11) Yella, A.; Lee, H. W.; Tsao, H. N.; Yi, C.; Chandiran, A. K.; Nazeeruddin, M. K.; Diau,
34
35 E. W. G.; Yeh, C. Y.; Zakeeruddin, S. M.; Grätzel, M. Porphyrin-Sensitized Solar Cells with
36
37 Cobalt (II/III)-Based Redox Electrolyte Exceed 12 Percent Efficiency. *Science* **2011**, *334*, 629–
38
39 634.
40
41

42
43 (12) Kuna, J. J.; Voitchovsky, K.; Singh, C.; Jiang, H.; Mwenifumbo, S.; Ghorai, P. K.;
44
45 Stevens, M. M.; Glotzer, S. C.; Stellacci, F. The Effect of Nanometre-Scale Structure on
46
47 Interfacial Energy. *Nat. Mater.* **2009**, *8*, 837–842.
48
49

50
51 (13) Schiffmann, F.; VandeVondele, J.; Hutter, J.; Wirz, R.; Urakawa, A.; Baiker, A.
52
53 Protonation-Dependent Binding of Ruthenium Bipyridyl Complexes to the Anatase(101)
54
55 Surface. *J. Phys. Chem. C* **2010**, *114*, 8398–8404.
56
57
58
59
60

1
2
3 (14) Yu, S.; Ahmadi, S.; Zuleta, M.; Tian, H.; Schulte, K.; Pietzsch, A.; Hennies, F.;
4 Weissenrieder, J.; Yang, X.; Göthelid, M. Adsorption Geometry, Molecular Interaction, and
5 Charge Transfer of Triphenylamine-Based Dye on Rutile TiO₂(110). *J. Chem. Phys.* **2010**, *133*,
6 224704.
7
8
9

10
11
12 (15) Marinado, T.; Hahlin, M.; Jiang, X.; Quintana, M.; Johansson, E. M. J.; Gabrielsson, E.;
13 Plogmaker, S.; Hagberg, D. P.; Boschloo, G.; Zakeeruddin, S. M.; Grätzel, M.; Siegbahn, H.;
14 Sun, L.; Hagfeldt, A.; Rensmo, H. Surface Molecular Quantification and Photoelectrochemical
15 Characterization of Mixed Organic Dye and Coadsorbent Layers on TiO₂ for Dye-Sensitized
16 Solar Cells. *J. Phys. Chem. C* **2010**, *114*, 11903–11910.
17
18
19
20
21
22
23

24 (16) Rienzo, A.; Mayor, L. C.; Magnano, G.; Satterley, C. J.; Ataman, E.; Schnadt, J.; Schulte,
25 K.; O'Shea, J. N. X-Ray Absorption and Photoemission Spectroscopy of Zinc Protoporphyrin
26 Adsorbed on Rutile TiO₂(110) Prepared by in Situ Electrospray Deposition. *J. Chem. Phys.*
27 **2010**, *132*, 084703.
28
29
30
31
32
33
34

35 (17) Kley, C. S.; Dette, C.; Rinke, G.; Cechal, J.; Jung, S. J.; Baur, M.; Dürr, M.;
36 Rauschenbach, S.; Giustino, F.; Stepanow, S.; Kern, K. Atomic-Scale Observation of
37 Multiconformational Binding and Energy Level Alignment of Ruthenium-Based Photosensitizers
38 on TiO₂ Anatase. *Nano Lett.* **2014**, *14*, 563-569.
39
40
41
42
43
44
45

46 (18) Sasahara, A.; Fujio, K.; Koide, N.; Han, L.; Onishi, H. STM Imaging of a Model Surface
47 of Ru(4,4''-Dicarboxy-2,2''-Bipyridine)₂(NCS)₂ Dye-Sensitized TiO₂ Photoelectrodes. *Surf. Sci.*
48 **2010**, *604*, 106–110.
49
50
51
52
53
54
55
56
57
58
59
60

1
2
3 (19) Marquet, P.; Andersson, G.; Snedden, A.; Kloo, L.; Atkin, R. Molecular Scale
4 Characterization of the Titania - Dye - Solvent Interface in Dye-Sensitized Solar Cells. *Langmuir*
5
6 **2010**, *26*, 9612–9616.
7
8

9
10
11 (20) Fukuma, T.; Higgins, M. J.; Jarvis, S. P. Direct Imaging of Lipid-Ion Network Formation
12 Under Physiological Conditions by Frequency Modulation Atomic Force Microscopy. *Phys. Rev.*
13
14 *Lett.* **2007**, *98*, 106101.
15
16

17
18
19 (21) Fukuma, T.; Ueda, Y.; Yoshioka, S.; Asakawa, H. Atomic-Scale Distribution of Water
20 Molecules at the Mica-Water Interface Visualized by Three-Dimensional Scanning Force
21
22 Microscopy. *Phys. Rev. Lett.* **2010**, *104*, 016101.
23
24
25

26
27 (22) Voitchovsky, K.; Kuna, J. J.; Contera, S. A.; Tosatti, E.; Stellacci, F. Direct Mapping of
28 the Solid–Liquid Adhesion Energy with Subnanometre Resolution. *Nat. Nanotechnol.* **2010**, *5*,
29
30 401–405.
31
32

33
34
35 (23) Zakeeruddin, S. M.; Nazeeruddin, M. K.; Humphry-Baker, R.; Pechy, P.; Quagliotto, P.;
36 Barolo, C.; Viscardi, G.; Grätzel, M. Design, Synthesis, and Application of Amphiphilic
37
38 Ruthenium Polypyridyl Photosensitizers in Solar Cells Based on Nanocrystalline TiO₂ Films.
39
40 *Langmuir* **2002**, *18*, 952–954.
41
42
43

44
45 (24) Wang, P.; Zakeeruddin, S. M.; Moser, J. E.; Nazeeruddin, M. K.; Sekiguchi, T.; Grätzel,
46
47 M. A Stable Quasi-Solid-State Dye-Sensitized Solar Cell with an Amphiphilic Ruthenium
48
49 Sensitizer and Polymer Gel Electrolyte. *Nat. Mater.* **2003**, *2*, 402–407.
50
51
52

1
2
3 (25) Rodahl, M.; Hook, F.; Krozer, A.; Brzezinski, P.; Kasemo, B. Quartz Crystal
4 Microbalance Setup for Frequency and Q-Factor Measurements in Gaseous and Liquid
5 Environments. *Rev. Sci. Instrum.* **1995**, *66*, 3924–3930.
6
7

8
9
10
11 (26) Rodahl, M.; Kasemo, B. Frequency and Dissipation-Factor Responses to Localized
12 Liquid Deposits on a QCM Electrode. *Sens. Actuators, B* **1996**, *37*, 111–116.
13
14

15
16
17 (27) Harms, H. A.; Tétreault, N.; Gusak, V.; Kasemo, B.; Grätzel, M. In-Situ Investigation of
18 Dye Adsorption on TiO₂ Films Using a Quartz Crystal Microbalance with Dissipation
19 Technique. *Phys. Chem. Chem. Phys.* **2012**, 9037–9040.
20
21
22

23
24
25 (28) Voïtchovsky, K. Phys. Rev. E Anharmonicity, solvation forces, and resolution in atomic
26 force microscopy at the solid-liquid interface. *Phys. Rev. E* **2013**, *88*, 022407.
27
28

29
30 (29) Cornell, W. D.; Cieplak, P.; Bayly, C. I.; Gould, I. R.; Merz, K. M.; Ferguson, D. M.;
31 Spellmeyer, D. C.; Fox, T.; Caldwell, J. W.; Kollman, P. A. [AMBER] a Second Generation
32 Force Field for the Simulation of Proteins, Nucleic Acids, and Organic Molecules. *J. Am. Chem.*
33 *Soc.* **1995**, *117*, 5179–5197.
34
35
36
37

38
39
40 (30) Bandura, A. V.; Kubicki, J. D. Derivation of Force Field Parameters for TiO₂ - H₂O
41 Systems From Ab Initio Calculations. *J. Phys. Chem. B* **2003**, *107*, 11072–11081.
42
43
44

45
46 (31) Case, D. A.; Darden, T. A.; Cheatham, T. E., III; Simmerling, C. L. AMBER 12 - Amber
47 Package. *University of California* **2012**.
48
49

50
51 (32) Bayly, C. I.; Cieplak, P.; Cornell, W.; Kollman, P. A. A Well-Behaved Electrostatic
52 Potential Based Method Using Charge Restraints for Deriving Atomic Charges: the RESP
53 Model. *J. Phys. Chem.* **1993**, *97*, 10269–10280.
54
55
56
57
58
59
60

1
2
3 (33) Frisch, M. J.; Trucks, G. W.; Schlegel, H. B.; Scuseria, G. E.; Robb, M. A.; Cheeseman,
4 J. R.; Scalmani, G. Gaussian 09, revision A. 1. *Gaussian Inc., Wallingford, CT* **2009**.

5
6
7
8
9 (34) Sushko, M. L.; Gal, A. Y.; Shluger, A. L. Interaction of Organic Molecules with the TiO₂
10 (110) Surface: Ab Initio Calculations and Classical Force Fields. *J. Phys. Chem. B* **2006**, *110*,
11 4853–4862.

12
13
14
15
16 (35) Jorgensen, W. L.; Tirado-Rives, J. The OPLS [Optimized Potentials for Liquid
17 Simulations] Potential Functions for Proteins, Energy Minimizations for Crystals of Cyclic
18 Peptides and Crambin. *J. Am. Chem. Soc.* **1988**, *110*, 1657–1666.

19
20
21
22 (36) Pastore, M.; Angelis, F. D. First-Principles Computational Modeling of Fluorescence
23 Resonance Energy Transfer in Co-Sensitized Dye Solar Cells. *J. Phys. Chem. Lett.* **2012**, *3*,
24 2146–2153.

25
26
27 (37) Grinter, D. C.; Nicotra, M.; Thornton, G. Acetic Acid Adsorption on Anatase TiO₂ (101).
28 *J. Phys. Chem. C* **2012**, *116*, 11643–11651.

29
30
31
32 (38) Polander, L. E.; Yella, A.; Curchod, B. F. E.; Ashari Astani, N.; Teuscher, J.; Scopelliti,
33 R.; Gao, P.; Mathew, S.; Moser, J. E.; Tavernelli, I.; Rothlisberger, U.; Grätzel, M.;
34 Nazeeruddin, M. K.; Frey, J. Towards Compatibility Between Ruthenium Sensitizers and Cobalt
35 Electrolytes in Dye-Sensitized Solar Cells. *Angew. Chem. Int. Ed.* **2013**, *52*, 8731–8735.

36
37
38 (39) Accelrys Software Inc., Discovery Studio Modeling Environment, Release 4.0, *San*
39 *Diego: Accelrys Software Inc.*, **2013**.

1
2
3 (40) Tétreault, N.; Heiniger, L.-P.; Stefik, M.; Labouchère, P. L.; Arsenault, É.; Nazeeruddin,
4 N. K.; Ozin, G. A.; Grätzel, M. Atomic Layer Deposition for Novel Dye-Sensitized Solar Cells.
5
6 *ECS Transactions* **2011**, *41*, 303-314.
7

8
9
10
11 (41) Yanada, K.; Chiba, K.; Yamaguchi, Y.; Yamamoto, H. Characteristics of Dye-Sensitized
12 Solar Cells Using Linear Sulfones as an Electrolyte Solvent. *Electrochim. Acta* **2012**, *79*, 163–
13
14 167.
15
16

17
18
19 (42) Chiba, K.; Ueda, T.; Yamaguchi, Y.; Oki, Y.; Saiki, F.; Naoi, K. Electrolyte Systems for
20 High Withstand Voltage and Durability II. Alkylated Cyclic Carbonates for Electric Double-
21 Layer Capacitors. *J. Electrochem. Soc.* **2011**, *158*, A1320.
22
23

24
25
26
27 (43) Hahlin, M.; Johansson, E. M. J.; Plogmaker, S.; Odelius, M.; Hagberg, D. P.; Sun, L.;
28 Siegbahn, H.; Rensmo, H. Electronic and Molecular Structures of Organic Dye/TiO₂ Interfaces
29 for Solar Cell Applications: a Core Level Photoelectron Spectroscopy Study. *Phys. Chem. Chem.*
30
31 *Phys.* **2010**, *12*, 1507.
32
33

34
35
36
37 (44) Schwartz, D. K. Mechanisms and Kinetics of Self-Assembled Monolayer Formation.
38
39 *Annu. Rev. Phys. Chem.* **2001**, *52*, 107–137.
40
41

42
43 (45) O'Regan, B.; Xiaoe, L.; Ghaddar, T. Dye Adsorption, Desorption, and Distribution in
44 Mesoporous TiO₂ Films, and Its Effects on Recombination Losses in Dye Sensitized Solar Cells.
45
46 *Energy Environ. Sci.* **2012**, *5*, 7203–7215.
47
48

49
50
51 (46) Gusak, V.; Heiniger, L.-P.; Graetzel, M.; Langhammer, C.; Kasemo, B. Time-Resolved
52 Indirect Nanoplasmonic Sensing Spectroscopy of Dye Molecule Interactions with Dense and
53
54 Mesoporous TiO₂ Films. *Nano. Lett.* **2012**, *12*, 2397–2403.
55
56
57
58
59
60

1
2
3 (47) Gusak, V.; Nkurunziza, E.; Langhammer, C.; Kasemo, B. Real-Time Adsorption and
4
5 Desorption Kinetics of Dye Z907 on a Flat Mimic of Dye-Sensitized Solar Cell TiO₂
6
7 Photoelectrodes. *J. Phys. Chem. C* **2014**, *118*, 17116-17122.
8
9
10
11
12
13
14
15
16
17
18
19
20
21
22
23
24
25
26
27
28
29
30
31
32
33
34
35
36
37
38
39
40
41
42
43
44
45
46
47
48
49
50
51
52
53
54
55
56
57
58
59
60

1
2
3 For Table of Contents Only
4
5
6

